

X-ray synchrotron emission from supernova remnants

Jean Ballet

DSM/DAPNIA/SAP, Bt 709, CEA Saclay, 91191 Gif sur Yvette Cedex, France

Abstract

X-ray synchrotron emission tells us of the highest energy reached by accelerated electrons. In a few supernova remnants (SN 1006, G347.3–0.5) this is the dominant form of X-ray radiation, but in most it is superposed to the dominant thermal emission. Thanks to the spectro-imaging capability of *Chandra* and *XMM-Newton*, X-ray synchrotron emission has now been unambiguously detected in most young supernova remnants (Cas A, Tycho, Kepler). It arises in a very thin shell (a few arcsecs) at the blast wave. The thinness of that shell (much broader in the radio domain) implies that the high energy electrons cool down very fast behind the shock. The magnetic field that one deduces from that constraint is more than 100 μG behind the shock.

Key words: Acceleration of particles, Magnetic fields, Cosmic rays, ISM: supernova remnants, X-rays

PACS: 98.38.Mz, 98.70.Sa

1 Introduction

The current paradigm is that the bulk of the cosmic-rays (up to the “knee” at 3×10^{15} eV) are accelerated at the blast waves generated by supernova explosions in our galaxy (Blandford and Eichler, 1987). Indeed supernova remnants (SNRs) are all non-thermal radio emitters, attesting of the presence of accelerated electrons at energies of 1 GeV or so in larger amounts than in the average interstellar medium. In most SNRs, the radio emission is limb-brightened, confirming that those accelerated electrons originate at the shock rather than in a central pulsar.

Email address: jballet@cea.fr (Jean Ballet).

The X-ray emission in those shell-type SNRs is usually mostly thermal (dominated by strong lines of heavy elements), but the synchrotron emission may extend up to the X-rays and contribute to the emission as well. In several cases, like SN 1006 (Koyama et al., 1995) and G347.3–0.5 (Koyama et al., 1997), the synchrotron component actually dominates the X-ray emission.

The slope of the X-ray synchrotron emission is always much steeper ($\alpha \simeq 1.5$) than that of the radio emission ($\alpha \simeq 0.5$). This indicates that the X-rays (emitted by electrons at energies > 1 TeV) probe the cut-off of the electron distribution, and can tell something about the limits of the shock acceleration mechanism. The open questions on which observations of X-ray synchrotron in SNRs may shed light are:

- How efficient is cosmic-ray acceleration in SNRs ? What is the energy density of accelerated particles ?
- What is the maximum energy of accelerated particles ?
- How large is the magnetic field ? Is it very turbulent ? Is it amplified ?

Unfortunately, not much is known about the synchrotron emission in the seven decades gap between the radio and the X-rays, partly because it is masked by other components (like infra-red emission by heated dust) and partly because it is simply very difficult to detect faint extended emission. Because of that ignorance, it is often assumed that the spectrum extends as a power law up to the cut-off, even though non linear acceleration models predict some concavity (Baring et al., 1999). The synchrotron emission has been detected in Cas A in the near infra-red (Jones et al., 2003), but this is associated with the bulk of the radio emission (near the interface with the ejecta), not with the relatively faint synchrotron emission from behind the blast wave discussed in the following sections.

In this review I report on recent observations of X-ray synchrotron emission in three young SNRs dominated by thermal emission from the ejecta (Cas A, Kepler and Tycho), and two older SNRs dominated by non-thermal emission (SN 1006 and G347.3–0.5). The inference is that the magnetic field just behind the blast wave is quite large (up to $200 \mu\text{G}$).

2 Observations at high angular resolution

Before it could be spatially resolved, the X-ray emission behind the blast wave in young SNRs was expected to be the thermal emission of the shocked ambient gas, distributed more or less evenly between the blast wave and the outer boundary of the ejecta. But the *Chandra* results challenged that pre-conception. The images of the continuum emission (4 to 6 keV) in Cas A (Gotthelf et al., 2001) and Tycho (Hwang et al., 2002) clearly show a very

thin X-ray rim at the blast wave. The apparent width of the rim is less than $4''$ or 2×10^{17} cm in Cas A, and appears to be twice lower at places. That X-ray rim runs all around both remnants, albeit in a broken manner (particularly in Cas A).

The 4 to 6 keV continuum emission in Kepler shows a very similar structure. Sharp (although not nearly as sharp) rims have also been observed in SN 1006 (Long et al., 2003; Bamba et al., 2003) and G347.3–0.5 (Lazendic et al., 2003). In those two SNRs, older and dominated by non-thermal emission, and contrary to the younger three mentioned above, there is no clear boundary behind which the thermal emission from the ejecta dominates. In G347.3–0.5, the thermal emission is not even detected at all. Also, because the non-thermal emission dominates, the energy range where its morphology can be studied is not restricted to the 4 to 6 keV band (SN 1006 is very faint in that band).

In Tycho, the rim clearly marks the outer boundary of the X-ray emission, so it is natural to think of it as a thin sheet covering the entire sphere, rather than a linear filament. This is supported by the observation of SN 1006, where the rim is definitely resolved, and much sharper outwards than inwards. The visual appearance of the rims in Cas A is much less regular. This is not a strong argument against the sheet geometry, however, because it is actually very reminiscent of the optical emission in older remnants like the Cygnus Loop, which is generally interpreted as due to a wrinkled sheet of emission (Hester, 1987). In keeping with this evidence, I will assume the rims are places where the sheet of emission at the blast wave is observed tangentially.

As noted by Berezhko and Völk (2004), since this is observed in projection the scale height of the spherical layer must be even smaller than the observed width. I argue in App. A that it should be 4.6 times smaller. This conclusion does not depend on the curvature radius of the sheet (it does not have to be equal to the SNR radius, it could even be negative – outwards), therefore it is quite robust. Exceptional geometrical conditions (like model B of Hester, 1987), normally associate a narrower rim with a larger brightness contrast between the rim and its surroundings. This should be testable statistically.

The brightness contrast of the X-ray continuum between at the rim and behind the rim is very large (typically 5). It is consistent with the thin sheet model in Cas A (Berezhko and Völk, 2004) and Tycho (Völk et al., 2005), but leaves little room for anything else. This implies that most of the volume between the blast wave and the interface with the ejecta is actually X-ray dark (in the continuum emission).

Another important observation is the nearly featureless nature of the spectrum (very faint lines are observed). In a thermal framework, this can be explained if ionization is very far out of equilibrium (Hwang et al., 2002, on Tycho). But

of course it is very natural if the spectrum of the rims is non-thermal. It is important to note in that respect that the line emission is not peaked at the rims. The brightness in the lines is essentially the same in a region behind the rims as on the rims in Cas A and Tycho. This suggests that the faint line emission comes from the entire volume between the blast wave and the bright ejecta, contrary to most of the continuum emission.

3 The nature of the X-ray emission behind the blast wave

The observed geometry is inconsistent with thermal models in a uniform medium which predict emission everywhere up to the interface, with only a slight maximum at the blast wave. This region is full of hot gas, which cannot cool down efficiently at those low densities, so it has to be entirely X-ray bright. Such a sharp decline of the X-ray emission behind the blast wave could be due to a recent density increase of the ambient gas, but it would have to be an extraordinary coincidence that this happens exactly at the same time all around the remnants in both Cas A and Tycho. In Cas A (a type II SN), having just hit a spherical wind shell could create such a condition, but it would result in a much slower shock, contrary to the observed proper motions (DeLaney and Rudnick, 2003).

Other known transient phenomena related to the thermal gas cannot explain the observations at all:

- Heavy element ionization affects the lines rather than the continuum.
- Electron heating by the ions predicts a hardening of the spectrum, but not a decrease in intensity.
- Dust destruction results in increasing emission.

The only other possible source of X-ray radiation is the accelerated particles. Non-thermal bremsstrahlung (by suprathermal electrons at 10 keV or so) could be an option. The density of targets (the thermal gas) does not decline steeply behind the shock, but collisional losses with the thermal electrons could be strong enough to get rid of the particles themselves as they are advected downstream. A gross estimate of the energy loss time for suprathermal electrons at energy E_{keV} in gas of electronic density n_e is $t_{\text{Coul}} = 4.9 \times 10^7 \text{ s } E_{\text{keV}}^{3/2} / n_e$. A more accurate formula may be found in Sturmer et al. (1997). Around 5 keV, this could be consistent with the observed width in Cas A (corresponding to an age of $2.5 \times 10^8 \text{ s } r/4$, where r is the total compression ratio) for a downstream gas density of $1.8 \text{ cm}^{-3} (r/4)^{-1}$. However, non-thermal bremsstrahlung must be associated with brighter thermal emission. In Cas A, Tycho or Kepler, no such bright thermal emission is observed associated with the X-ray rims. With an interstellar column density N_{H} of several 10^{21} cm^{-2} , it is conceivable

that the thermal gas could hide at low temperature around 1 or 2×10^6 K. Such a low temperature is actually predicted by strongly non linear acceleration models (Decourchelle et al., 2000). SN 1006, on the other hand, has much lower $N_H \simeq 7 \times 10^{20} \text{ cm}^{-2}$ (Dubner et al., 2002). The soft thermal emission (in particular the O K lines) is clearly seen there at the same place as the harder X-ray rims. However it is not brighter than the non-thermal emission at all, which eliminates the possibility that the non-thermal continuum could be a tail of the thermal emission.

The most natural remaining option is synchrotron emission by high energy electrons. Here again, advection of the particles and the magnetic field (with only slight adiabatic losses) cannot explain the very sharp drop behind the shock. On the other hand, the particles may lose their energy radiatively fast enough as they are advected (so that their synchrotron emission is shifted below the X-ray range) to explain a very thin emission region if the magnetic field is large enough (Ballet, 2003; Vink and Laming, 2003). In Sect. 4 I develop the consequences of that interpretation.

The synchrotron interpretation implies also that the density (or the temperature) of the ambient gas must be low enough that it does not contribute significantly to the X-ray emission. This is possible if n (shocked) $< 0.15 \text{ cm}^{-3}$ in Kepler (Cassam-Chenaï et al., 2004a). The constraint for Tycho is probably a little less severe. Another prediction is that the radio emission should be much broader (not so peaked at the rims), because the GeV electrons emitting the radio are not affected by losses. This is indeed what is observed in Cas A (Vink and Laming, 2003). In SN 1006 (Long et al., 2003, Fig. 4), it is true as well that the non-thermal X-ray emission (above 1.2 keV) is much sharper than the radio emission. The radio is never more peaked than the X-ray emission below 0.8 keV, which is mostly thermal (O K lines). In Tycho on the other hand, a radio peak just behind the blast wave (associated with the X-ray rim) seems to exist (Dickel et al., 1991). This is difficult to understand in the synchrotron interpretation of the X-rays.

Recently, Lyutikov and Pohl (2004) suggested that the narrow rims could mark the interface between the ejecta and the shocked ambient gas, rather than the blast wave. Indeed it is relatively natural to reach high magnetic fields there. However, I do not think this interpretation is tenable for three reasons:

- Optical $H\alpha$ observations show filaments at the same distance from the SNR center as the X-ray rims (although not coincident with them). The line shape indicates that a fast (originally ionized) and a slow (originally neutral) population exist there. It is hard to imagine what could cause this far from a shock.
- No strong metal lines are observed immediately behind the rims, even in SN Ia (Tycho), where no hydrogen envelope should exist just behind the

interface.

- One would have to find another explanation for the bulk of the radio emission (far behind the X-ray rims), which is currently interpreted as originating in the high magnetic fields at the interface.

4 Physical conditions behind the blast wave

Quantitatively, the interpretation of the X-ray rims as synchrotron goes as follows. The synchrotron cooling time depends on the magnetic field and the electron's energy as $t_{\text{cool}} = 6.37 \times 10^8 B_{\text{mG}}^{-2} E_{\text{erg}}^{-1}$ s. Since the characteristic frequency at which an electron radiates is $\nu_{\text{sync}} = 1.82 \times 10^{15} B_{\text{mG}} E_{\text{erg}}^2$ Hz, the cooling time may be expressed as a function of the frequency at which the rims are observed.

$$t_{\text{cool}} = 5.5 \times 10^7 B_{\text{mG}}^{-3/2} \nu_{\text{keV}}^{-1/2} \text{ s} \quad (1)$$

Two effects (expected to be of the same order at the maximum energy reached by loss-limited electrons) combine to set the scale height of the emission behind the shock: advection (Ballet, 2003; Vink and Laming, 2003; Bamba et al., 2003) and diffusion (Berezhko et al., 2003; Yamazaki et al., 2004).

$$l_{\text{adv}} = t_{\text{cool}} v_{\text{sh}} / r = 1.8 \times 10^3 B_{\text{mG}}^{-3/2} \nu_{\text{keV}}^{-1/2} v_{1000} / r \text{ pc} \quad (2)$$

$$l_{\text{dif}} = \sqrt{\kappa_{\text{d}} t_{\text{cool}}} = 1.2 \times 10^{-3} B_{\text{mG}}^{-3/2} \text{ pc} \quad (3)$$

$$l_{\text{adv}} / l_{\text{dif}} = 1.5 \nu_{\text{keV}}^{-1/2} v_{1000} / r \quad (4)$$

where v_{sh} is the shock speed, $v_{1000} = v_{\text{sh}} / (1000 \text{ km/s})$, r is the total compression ratio and $\kappa_{\text{d}} = c / (3e) E / B$ is the downstream diffusion coefficient in the Bohm limit.

The observed characteristics of the five young shell-type SNRs for which enough data exists are summarized in Table 1, together with the required magnetic field. The ratio $l_{\text{adv}} / l_{\text{dif}}$ is always estimated assuming a compression ratio of 4. If the compression ratio is larger (as predicted by non-linear acceleration models), then l_{adv} will be smaller but the magnetic field estimate (from l_{dif}) won't change.

Overall, this interpretation imposes $B \simeq 200 \mu\text{G}$ downstream in the three youngest SNRs. It is a very important result because it provides observational evidence for the idea (Bell and Lucek, 2001) that diffusively accelerated particles streaming ahead of the shock are able to generate a turbulent magnetic field larger than the original ordered field (which cannot be larger than a few μG in such surroundings). This is potentially the key for breaking the

Name	Distance	Shock speed	Age	Cut-off frequency
Cas A	3.4 kpc ¹	5200 km/s ²	320 yr ? ⁴	1.2 keV ³
Kepler	4.8 kpc ⁵	5400 km/s ⁶	400 yr	0.9 keV ⁸
Tycho	2.3 kpc ⁹	4600 km/s ¹⁰	430 yr	0.29 keV ¹¹
SN 1006	2.2 kpc ¹²	2900 km/s ¹³	1000 yr	3 keV ¹⁵
G347.3–0.5	1.3 kpc ¹⁶	4000 km/s ? ¹⁷	1620 yr ? ¹⁹	2.6 keV ¹⁸

Name	Obs. freq.	$l_{\text{adv}}/l_{\text{dif}}$	Projected width	Magnetic field
Cas A	5 keV	0.88	0.05 pc (3'') ³	230 μG
Kepler	5 keV	0.92	0.07 pc (3'') ⁷	180 μG
Tycho	5 keV	0.78	0.05 pc (4'') ¹¹	250 μG
SN 1006	2 keV	0.78	0.2 pc (20'') ¹⁴	87 μG
G347.3–0.5	2 keV	1.06	0.25 pc (40'') ¹⁸	79 μG

Table 1

Characteristics of the non-thermal emission behind the blast wave in young SNRs. The cut-off frequency is rather uncertain. The magnetic field is always estimated from equating l_{dif} (Eq. 3) and the projected width divided by 4.6 (App. A), even when $l_{\text{adv}}/l_{\text{dif}}$ (from Eq. 4) is formally larger than 1.

References: ¹ Reed et al. (1995), ² Vink et al. (1998), ³ Vink and Laming (2003) from a fit to the spectrum of the whole SNR, ⁴ Ashworth (1980), ⁵ Reynoso and Goss (1999), ⁶ Hughes (1999)+distance, ⁷ Decourchelle (private communication), ⁸ Cassam-Chenai et al. (2004a) in the southeast, ⁹ Smith et al. (1991), ¹⁰ Hughes (2000), ¹¹ Hwang et al. (2002), ¹² Winkler et al. (2003), ¹³ Ghavamian et al. (2002) in the northwest, ¹⁴ Bamba et al. (2003) in the northeast, ¹⁵ Rothenflug et al. (2004) in the northeast, ¹⁶ Cassam-Chenai et al. (2004b), ¹⁷ from $v = \lambda r/t$ taking the expansion parameter $\lambda = 2/3$, ¹⁸ Lazendic et al. (2003) in the northwest, ¹⁹ Wang et al. (1997)

Lagage and Cesarsky (1983) limit and accelerating protons and heavier ions (not limited by radiative losses) up to the 'knee' of the cosmic-ray distribution at $3 \cdot 10^{15}$ eV. An observational consequence is that it predicts weak inverse Compton emission in the TeV range, because the density of accelerated electrons (for a given synchrotron emission) is much lower than estimated from a 'standard' compressed field of 10 μG or so.

A somewhat puzzling aspect is the geometry of the acceleration with respect to the magnetic field. In G347.3–0.5 and Kepler, the very large asymmetry in the X-ray image is probably due to variations of the exterior conditions (ambient density), so it is difficult to infer anything on the geometry. In SN 1006, the non-thermal emission is very clearly bipolar. The very faint X-ray emission from the center of the remnant above 2 keV led Rothenflug et al.

(2004) to conclude that the non-thermal X-rays are emitted in two polar caps. This is coherent with theoretical ideas (Völk et al., 2003) that acceleration works better where the magnetic field was originally parallel (to the shock velocity). Unfortunately, that nice picture is not at all what we see in Cas A (Hwang et al., 2004) and Tycho (Hwang et al., 2002) where the non-thermal X-ray rims seem to run all around the remnants. The main differences between those two and SN 1006 are the shock velocity and the ambient density (both lower in SN 1006). It may be that somehow the faster acceleration at larger shock velocities can work whatever the magnetic orientation, but a quantitative explanation does not exist yet.

5 The shock precursor in the ambient gas

The principle of diffusive acceleration predicts that the accelerated particles and the magnetic field should also be present some distance ahead of the shock. This means that synchrotron emission should be observed at some level upstream of the blast wave.

The absence of such a precursor in the radio range (an upper limit on its width) implies an upper limit on the diffusion coefficient at the energy of electrons which radiate in the radio. This is equivalent to a lower limit on the turbulent field which is larger than the ordinary interstellar turbulence. This argument led Achterberg et al. (1994) to conclude that accelerated particles could indeed generate the turbulent field which is required for acceleration to be a fast process.

Because the diffusion coefficient (for a given level of turbulence) increases with energy, X-ray observations (corresponding to electron energies 10^4 times larger than radio observations) provide a much more stringent constraint. In Cas A and Tycho, the radial profile of the X-ray emission appears symmetric, so one might think that the width used above may be used as an upper limit to the size of the precursor.

It is not so, though, because the shock compression necessarily results in compression of the magnetic field. Assuming isotropic magnetic turbulence upstream and shock compression by a factor r_{sub} , the magnetic field downstream may be larger than upstream by a factor $r_B = \sqrt{(1 + 2r_{\text{sub}}^2)}/3$, and the synchrotron emission by approximately r_B^Γ (because increasing B moves the spectrum both up and to larger frequencies), where Γ is the X-ray photon index (typically 2.5 to 3). r_{sub} here is the compression ratio at the gas subshock. It is always lower than 4, and decreases when the total compression ratio r increases.

In SN 1006, there is no evidence of a precursor either. Long et al. (2003) give a very stringent upper limit of 1.5% of the postshock level to the X-ray brightness about $20''$ (or 0.2 pc) upstream. They argue that this could be explained with a large magnetic field jump (larger than 4), possibly due to magnetic field amplification at the shock. Bamba et al. (2003) argue that it can be due to a perpendicular (to the shock normal) magnetic field. But Rothenflug et al. (2004), on the basis of the overall geometry of the X-ray emission, show that this cannot be true (the bright limbs must be polar caps rather than an equatorial belt). Berezhko et al. (2003) show that the observed profiles are compatible with the expected emissivity jump for a turbulent field ($r_B^\Gamma = 12.5$ with $r_{\text{sub}} = 3.6$ and $\Gamma = 2.3$), plus the intensity decrease outwards on the diffusive scale height. In other words, this constrains the upstream diffusive scale height for electrons emitting 1.5 keV X-rays to be lower than 0.12 pc or so. Assuming Bohm diffusion, the upstream scale height κ_u/v_{sh} deduced from Table 1, dividing B by r_B and deducing E corresponding to emission at 2 keV, is 0.08 pc. This is close enough that the precursor should be detectable in the near future.

Acknowledgements

I acknowledge constant discussion with A. Decourchelle, and many discussions on particle acceleration with D. Ellison, E. Parizot, Y. Gallant and A. Marcowith. I am also indebted to the referees who helped me understand what was not obvious in the picture I present.

A Projection of a thin sheet along the line of sight

Let r be the distance to the center of a sphere in units of the sphere's radius R_s , and ρ the distance to the center of the disk it projects onto a plane (in the same units). The projection of a spherically symmetric emissivity $\mathcal{E}(r)$ onto that plane results in an axisymmetric brightness profile

$$\mathcal{B}(\rho) = 2 R_s \int_0^{\sqrt{1-\rho^2}} \mathcal{E}(r) dz \quad (\text{A.1})$$

$$r^2 = \rho^2 + z^2 \quad (\text{A.2})$$

where z is the coordinate perpendicular to the plane.

If the emissivity is concentrated near $r = 1$, it may be written $\mathcal{E}(r) = f(x)$ where $x = (1 - r)/a$, f is the functional form of the decrease and a is the

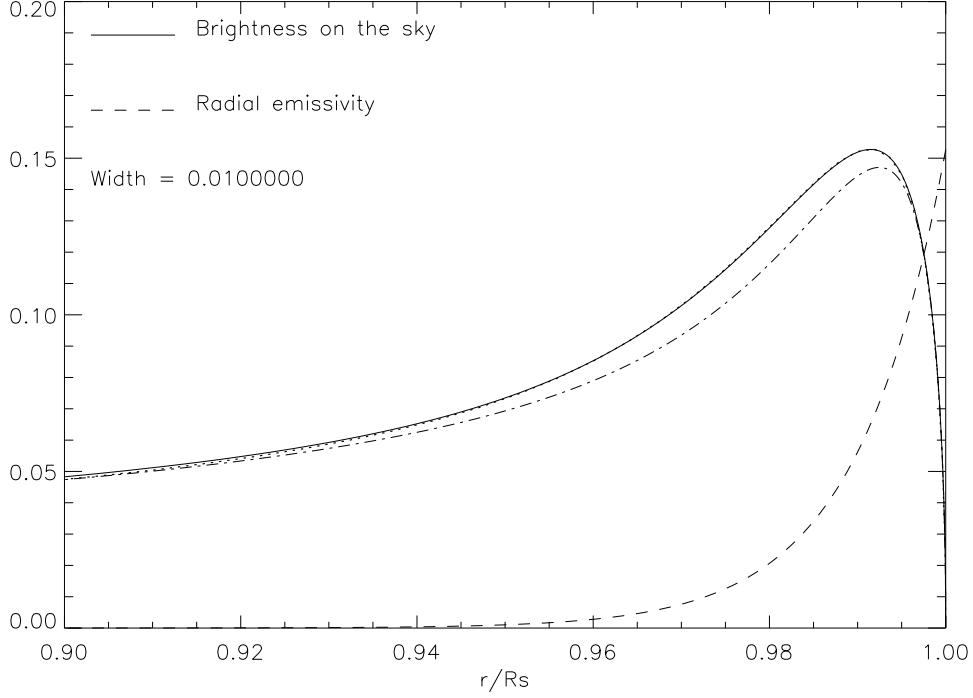


Fig. A.1. Emissivity profile exponentially decreasing inward (Eq. A.8 with $a = 0.01$, dashed line) compared with brightness profile projected onto the sky (Eq. A.1, solid line). The brightness units are $R_s \times$ the emissivity at the shock, where R_s is the shock radius. On that scale, the brightness at the center of the disk is 0.02. The emissivity profile was scaled down (for illustration purposes) to the same maximum. The dotted line (barely distinguishable from the solid one) is the result of the thin sheet approximation (Eq. A.5). The dash-dotted line is Eq. 6 of Berezhko and Völk (2004).

scale height (in units of R_s). Defining $y = (1 - \rho)/a$ and $u = z/\sqrt{2a}$, r may be developed for ρ close to 1 at order 2 in powers of z to give

$$r \simeq \rho \left(1 + \frac{z^2}{2\rho^2} \right) \quad (\text{A.3})$$

$$\frac{1-r}{a} \simeq y - u^2 \quad (\text{A.4})$$

$$\mathcal{B}(\rho) \simeq 2 R_s \sqrt{2a} \int_0^{\sqrt{y}} f(y - u^2) du \quad (\text{A.5})$$

Eq. A.5 is of the form $\mathcal{B}(\rho) = 2R_s\sqrt{2a}g(y)$. It always has the same functional form in terms of y near the edge of the disk (whatever the width a). In the same limit of small a , the brightness toward the center of the sphere is

$$\mathcal{B}(0) = 2 R_s \int_0^1 \mathcal{E}(r) dr \quad (\text{A.6})$$

$$\mathcal{B}(0) \simeq 2 R_s a \int_0^\infty f(x) dx \quad (\text{A.7})$$

The formulae above may be quantified in the special case of exponential decrease, shown on Fig. A.1.

$$\mathcal{E}(r) = \exp\left(\frac{r-1}{a}\right) \quad (\text{A.8})$$

$$\mathcal{B}(\rho) \simeq 2 R_s \sqrt{2a} e^{-y} \int_0^{\sqrt{y}} \exp(u^2) du \quad (\text{A.9})$$

Then the maximum of $g(y)$ occurs at $y_0 = 0.854$ where it reaches $g_0 = 0.541$. $g(y)$ decreases inwards to half that value at $y_1 = 4.685$. $g(y)$ decreases outwards to half that value at $y_2 = 0.082$. The full width at half maximum is thus $(y_1 - y_2) a = 4.603 a$. For comparison, the FWHM of the exponential itself is $\log 2 a = 0.693 a$. The ratio between the brightness at the center of the sphere and at maximum is $\mathcal{B}(0)/\mathcal{B}_{\max} = \sqrt{a/2/g_0} = 1.307\sqrt{a}$. The explicit (non-integral) approximation proposed by Berezhko and Völk (2004) is less accurate in representing the peak, but correctly represents the profile toward the center of the sphere (Eq. A.9 doesn't). Note that the difference with the value $7 a$ given for the width by Berezhko and Völk (2004) is mostly due to a different definition (they consider the width at $1/e$ of the maximum).

References

- Achterberg, A., Blandford, R. D., Reynolds, S. P., 1994. Evidence for enhanced mhd turbulence outside sharp-rimmed supernova remnants. *A&A* 281, 220–230.
- Ashworth, W. B., 1980. A probable flamsteed observations of the cassiopeia-a supernova. *J. Hist. Astr.* 11, 1.
- Ballet, J., 2003. X-ray observations of supernova remnants. In: Arthur, J., Henney, W. (Eds.), *Winds, bubbles and explosions (Patzcuaro 2002)*. Vol. 15. *Rev. Mex. de Astronomia y Astrofisica (Conferencias)*, pp. 237–242.
- Bamba, A., Yamazaki, R., Ueno, M., Koyama, K., 2003. Small-scale structure of the sn 1006 shock with chandra observations. *ApJ* 589, 827–837.
- Baring, M. G., Ellison, D. C., Reynolds, S. P., Grenier, I. A., Goret, P., 1999. Radio to gamma-ray emission from shell-type supernova remnants: Predictions from nonlinear shock acceleration models. *ApJ* 513, 311–338.

- Bell, A. R., Lucek, S. G., 2001. Cosmic ray acceleration to very high energy through the non-linear amplification by cosmic rays of the seed magnetic field. *MNRAS* 321, 433–438.
- Berezhko, E. G., Ksenofontov, L. T., Völk, H. J., 2003. Confirmation of strong magnetic field amplification and nuclear cosmic ray acceleration in sn 1006. *A&A* 412, L11–L14.
- Berezhko, E. G., Völk, H. J., 2004. Direct evidence of efficient cosmic ray acceleration and magnetic field amplification in cassiopeia a. *A&A* 419, L27–L30.
- Blandford, R. D., Eichler, D., 1987. Particle acceleration at astrophysical shocks - a theory of cosmic-ray origin. *Phys. Repts* 154, 1–75.
- Cassam-Chenaï, G., Decourchelle, A., Ballet, J., Hwang, U., Hughes, J. P., Petre, R., 2004a. Xmm-newton observation of kepler’s supernova remnant. *A&A* 414, 545–558.
- Cassam-Chenaï, G., Decourchelle, A., Ballet, J., Sauvageot, J. L., Dubner, G., Giacani, E., 2004b. Xmm-newton observations of the supernova remnant rx j1713.7-3946 and its central source observations of snr rx j1713.7-3946. *A&A* 427, 199–216.
- Decourchelle, A., Ellison, D. C., Ballet, J., 2000. Thermal x-ray emission and cosmic-ray production in young supernova remnants. *ApJ* 543, L57–L60.
- DeLaney, T., Rudnick, L., 2003. The first measurement of cassiopeia a’s forward shock expansion rate. *ApJ* 589, 818–826.
- Dickel, J. R., van Breugel, W. J. M., Strom, R. G., 1991. Radio structure of the remnant of tycho’s supernova (sn 1572). *AJ* 101, 2151–2159.
- Dubner, G. M., Giacani, E. B., Goss, W. M., Green, A. J., Nyman, L. A., 2002. The neutral gas environment of the young supernova remnant sn 1006 (g327.6+14.6). *A&A* 387, 1047–1056.
- Ghavamian, P., Winkler, P. F., Raymond, J. C., Long, K. S., 2002. The optical spectrum of the sn 1006 supernova remnant revisited. *ApJ* 572, 888–896.
- Gotthelf, E. V., Koralesky, B., Rudnick, L., Jones, T. W., Hwang, U., Petre, R., 2001. Chandra detection of the forward and reverse shocks in cassiopeia a. *ApJ* 552, L39–L43.
- Hester, J. J., 1987. A sheet description of the emission from middle-aged supernova remnants. *ApJ* 314, 187–202.
- Hughes, J. P., 1999. The extraordinarily rapid expansion of the x-ray remnant of kepler’s supernova (sn 1604). *ApJ* 527, 298–309.
- Hughes, J. P., 2000. The expansion of the x-ray remnant of tycho’s supernova (sn 1572). *ApJ* 545, L53–L56.
- Hwang, U., Decourchelle, A., Holt, S. S., Petre, R., 2002. Thermal and nonthermal x-ray emission from the forward shock in tycho’s supernova remnant. *ApJ* 581, 1101–1115.
- Hwang, U., Laming, J. M., Badenes, C., Berendse, F., Blondin, J., et al., 2004. A million second chandra view of cassiopeia a. *ApJ* 615, L117–L120.
- Jones, T. J., Rudnick, L., DeLaney, T., Bowden, J., 2003. The identification of infrared synchrotron radiation from cassiopeia a. *ApJ* 587, 227–234.

- Koyama, K., Kinugasa, K., Matsuzaki, K., Nishiuchi, M., Sugizaki, M., Torii, K., Yamauchi, S., Aschenbach, B., 1997. Discovery of non-thermal x-rays from the northwest shell of the new snr rx j1713.7-3946: The second sn 1006? PASJ 49, L7–L11.
- Koyama, K., Petre, R., Gotthelf, E. V., Hwang, U., Matsuura, M., Ozaki, M., Holt, S. S., 1995. Evidence for shock acceleration of high-energy electrons in the supernova remnant sn:1006. *Nature* 378, 255–258.
- Lagage, P. O., Cesarsky, C., 1983. The maximum energy of cosmic rays accelerated by supernova shocks. *A&A* 125, 249–257.
- Lazendic, J. S., Slane, P. O., Gaensler, B. M., Plucinsky, P. P., Hughes, J. P., Galloway, D. K., Crawford, F., 2003. X-ray observations of the compact central object in supernova remnant g347.3-0.5. *ApJ* 593, L27–L30.
- Long, K. S., Reynolds, S. P., Raymond, J. C., Winkler, P. F., Dyer, K. K., Petre, R., 2003. Chandra ccd imagery of the northeast and northwest limbs of sn 1006. *ApJ* 586, 1162–1178.
- Lyutikov, M., Pohl, M., 2004. The origin of nonthermal x-ray filaments and tev emission in young supernova remnants. *ApJ* 609, 785–796.
- Reed, J. E., Hester, J. J., Fabian, A. C., Winkler, P. F., 1995. The three-dimensional structure of the cassiopeia a supernova remnant. i. the spherical shell. *ApJ* 440, 706–721.
- Reynoso, E. M., Goss, W. M., 1999. A new determination of the distance to kepler’s supernova remnant. *AJ* 118, 926–929.
- Rothenflug, R., Ballet, J., Dubner, G., Giacani, E., Decourchelle, A., Ferrando, P., 2004. Geometry of the non-thermal emission in sn 1006. azimuthal variations of cosmic-ray acceleration. *A&A* 425, 121–131.
- Smith, R. C., Kirshner, R. P., Blair, W. P., Winkler, P. F., 1991. Six balmer-dominated supernova remnants. *ApJ* 375, 652–662.
- Sturmer, S. J., Skibo, J. G., Dermer, C. D., Mattox, J. R., 1997. Temporal evolution of nonthermal spectra from supernova remnants. *ApJ* 490, 619–632.
- Vink, J., Bloemen, H., Kaastra, J. S., Bleeker, J. A. M., 1998. The expansion of cassiopeia a as seen in x-rays. *A&A* 339, 201–207.
- Vink, J., Laming, J. M., 2003. On the magnetic fields and particle acceleration in cassiopeia a. *ApJ* 584, 758–769.
- Völk, H. J., Berezhko, E. G., Ksenofontov, L. T., 2003. Variation of cosmic ray injection across supernova shocks. *A&A* 409, 563–571.
- Völk, H. J., Berezhko, E. G., Ksenofontov, L. T., 2005. Magnetic field amplification in tycho and other shell-type supernova remnants. *astro-ph/0409453*.
- Wang, Z. R., Qu, Q. Y., Chen, Y., 1997. Is rx j1713.7-3946 the remnant of the ad393 guest star? *A&A* 318, L59–L61.
- Winkler, P. F., Gupta, G., Long, K. S., 2003. The sn 1006 remnant: Optical proper motions, deep imaging, distance, and brightness at maximum. *ApJ* 585, 324–335.
- Yamazaki, R., Yoshida, T., Terasawa, T., Bamba, A., Koyama, K., 2004. Constraints on the diffusive shock acceleration from the nonthermal x-ray thin

shells in sn 1006 ne rim. A&A 416, 595–602.